Journal of Solid State Chemistry 184 (2011) 1135–1140

Contents lists available at ScienceDirect

Journal of Solid State Chemistry

journal homepage: www.elsevier.com/locate/jssc

$CdTe@Cu(OH)_2$ nanocomposite: Aqueous synthesis and characterization

M.S. Abd El-sadek [a,b,*], S. Moorthy Babu [b]

[a] Nanomaterial Laboratory, Physics Department, Faculty of Science, South Valley University, Qena 83523, Egypt
[b] Crystal Growth Centre, Anna University Chennai, Chennai 600025, India

ARTICLE INFO

Article history:
Received 27 September 2010
Received in revised form
24 January 2011
Accepted 2 March 2011
Available online 21 March 2011

Keywords:
CdTe nanocrystals
Nanocomposites
Mercaptoacetic Acid
Optical and magnetic properties
FT-IR spectroscopy

ABSTRACT

$CdTe@Cu(OH)_2$ nanocomposites were synthesized in aqueous solution by a seed-mediated growth approach. The effect of refluxing time and the concentration of Cu^{2+} on the preparation of these samples were measured using UV–visible absorption and photoluminescence analysis. The emission peak of the synthesized nanocomposites ($CdTe@Cu(OH)_2$) was shifted from 605 (CdTe seed) to 621 nm. The size of CdTe nanoparticles were averaged about 3.22 nm, and the $CdTe@Cu(OH)_2$ nanocomposites were averaged as 5.19 nm. The synthesized $CdTe@Cu(OH)_2$ nanocomposite were characterized with XRD, EDAX, TEM, FT-IR, EPR, and thermal analysis (TG/DTG curves). The results indicate that as-prepared nanoparticles with core/shell structure exhibit interesting optical properties.

1. Introduction

Nanocomposites are a special class of materials originating from suitable combinations of two or more such nanoparticles or nanosized objects in some suitable technique, resulting in materials having unique physical properties and wide application potential in diverse areas. Novel properties of nanocomposites can be derived from the successful combination of the characteristics of parent constituents into a single material. Materials scientists very often handle such nanocomposites, which are an effective combination of two or more inorganic nanoparticles [1]. Nanocomposite structures have been used to create optically functional materials. By incorporating semiconductor nanoparticles into polymer, glass, or ceramic matrix materials, many of their interesting optical properties including absorption, fluorescence, luminescence, and nonlinearity may be studied. In these systems, very small particle sizes enhance the optical properties, while the matrix materials act to stabilize the particle size and growth. Nanocomposite structures provide a new method to improve the processability and stability of these materials with interesting optical properties [2–4].

Metals have been grown on magnetic metal cores [5] and vice versa, [6] to form core–shell structures, leading to changes in magnetic, optical, and chemical properties compared to those of the individual components [5,6]. Enhancement or modifications of properties resulting from the core–shell structures are becoming more common. The isolation of the core from the surroundings can be used to create objects with fundamentally different properties to those of the bare nanocrystal. For example, the coating may be used to passivate the core chemically in order to modify its optical properties, or it may be used as a size-selective membrane for catalytic processes at the core surface [7]. A further possibility is the construction of electronic components and devices, by using the core-shell structure to create nanoscale objects with specific electrical functionality [8]. More recently, coating a semiconductor layer on magnetic nanocrystals was used to create luminescent/magnetic composite nanomaterials [3,4,9,10].

$Cu(OH)_2$ with an orthorhombic structure have been studied extensively in the past several years. Polycrystalline $Cu(OH)_2$ nanowires and nanoribbons were synthesized through a two-step wet chemical route [11,12], or by the interaction between a copper complex and NaOH at the aqueous-organic interface [13], or prepared in aqueous solution of ammonia using Cu_2S nanowires as precursors [14]. Single-crystalline $Cu(OH)_2$ nanoribbon and nanotubes were successfully synthesized by surface oxidation of copper foil in alkaline solutions [15] or anion exchange reaction using NaOH solution [16]. A simple, clean, and effective route for fabrication of large area $Cu(OH)_2$ nanostructured films were reported [17]. The reported $Cu(OH)_2$ nanoneedle and nanotube arrays were electrochemically synthesized by anodization of a copper foil in an aqueous solution of KOH.

$CdTe@Cu(OH)_2$ nanocomposites were synthesized by a seed-mediated growth approach composed of a fluorescent nanocrystals, CdTe as core, and a magnetic metal hydroxides, $Cu(OH)_2$ as shell.

* Corresponding author Present address: Department of Chemical Physics, Lund University, SE-22 100 Lund, Sweden.
Fax: +2 096 5211279.
E-mail addresses: el_sadek_99@yahoo.com, el_sadek_99@email.com, Mahmmoud.Sayed@chemphys.lu.se (M.S. Abd El-sadek).

0022-4596/$ - see front matter © 2011 Elsevier Inc. All rights reserved.
doi:10.1016/j.jssc.2011.03.002

Nanoparticles show unique optical properties, and copper hydroxides have specific properties such as electrochemical activity, magnetism and catalysis. These nanocomposites were water-soluble and show good optical properties. The synthesis procedure was described and the composite nanomaterials were characterized by UV–visible absorption, photoluminescence, X-ray diffraction, energy-dispersive X-ray analysis (EDAX), transmission electron microscopy (TEM), FT-IR spectroscopy, electron paramagnetic resonance (EPR), and thermal analysis (TG/DTG curves).

2. Experimental procedure

Preparation of CdTe@$Cu(OH)_2$ nanocomposite was performed using the following procedure as shown in Fig. 1.

All chemicals were purchased from Central Drug House (P) Ltd (CDH) and were of the highest purity available (99.9%). De-ionized water obtained from a Millipore Milli-Q Plus purification system was used in all experiments. MAA-capped CdTe nanoparticles were synthesized as reported in our previous work [3,4,18] and Cu^{2+} was added as copper chloride solution. Aqueous solution of (0.01 M) $CuCl_2 \cdot 2H_2O$ was injected by multiple-steps to the colloidal solution for formation of the $Cu(OH)_2$ shell on the CdTe nanocrystals. Under the alkaline conditions with the stabilizer (MAA), Cu^{2+} hydrolyzed and formed $Cu(OH)_2$. In a typical synthesis, 5 ml of 0.01 M $CuCl_2 \cdot 2H_2O$ aqueous solutions was added into 250 ml (1 mM) CdTe colloidal solution (MAA, 5 mM), and then adjusted to pH ($\approx$11.2) with 2 M KOH. The solution was placed in a three-necked flask and was heated to 90 °C with condenser attached to reflux for a set time. In the presence of mercaptoacetic acid (MAA) and weak basic solution, Cu^{2+} hydrolyzes and forms hydroxide deposits on the surface of CdTe nanocrystals. The refluxing process with Cu^{2+} can be repeated several times for coating more hydroxides on CdTe nanocrystals. The $CuCl_2 \cdot 2H_2O$ solution was multi-injected for avoiding the agglomeration of the particles caused by the sudden increasing of ions in strength. Typically, at the reflux time of 6 h, 5 ml of 0.01 M $CuCl_2 \cdot 2H_2O$ solution was injected into the 250 ml CdTe colloidal solution (Sample S_0) and further refluxed 1 h (Sample S_1, was taken from this stage), and then another 5 ml of 0.01 M $CuCl_2 \cdot 2H_2O$ solution was injected and the refluxing was continued for 1 h, then, the final sample (S_2) was obtained. The size of CdTe core was controlled by the reflux time of CdTe colloidal solution. The $Cu(OH)_2$ shell thickness was controlled by the amount of Cu in the solution. The method of size selective precipitation was used to isolate the nanocomposites. As-prepared colloid samples were diluted for optical characterization and precipitated by 2-propanol for other characterization studies. The resulting composite nanomaterials were characterized by UV–visible absorption, Photoluminescence, XRD, EDAX, TEM, FT-IR, EPR, and thermal analysis.

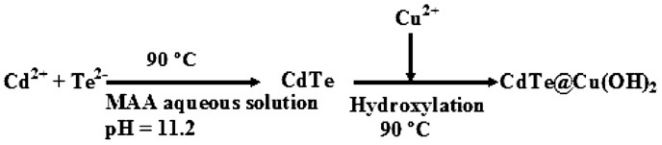

Fig. 1. Schematic of aqueous synthesis route for CdTe@$Cu(OH)_2$ nanocomposite.

UV–visible absorption analysis was carried out using a Cary 5E UV–vis–NIR spectrophotometer. Photoluminescence measurements were performed at room temperature using JY Fluorolog-3-11 spectrofluorometer (at the excitation wavelength λ_{exc}=460 nm). Samples were prepared by diluting colloidal solutions with water. All optical measurements were performed at room temperature under ambient conditions. X-ray powder diffraction analysis was carried out with a Philips X'Pert PRO diffractometer with Cu$K\alpha$ (λ=0.15406 nm) radiation and EDAX was performed on EDS Noran System Six (Thermo Electron Corporation). Transmission electron microscopy (TEM) was performed using a JEM-1011 (accelerating voltage of 100 kV) in order to analyze the size and also to confirm the formation of the core/shell structure. IR spectra were recorded with a Perkin Elmer FT-IR spectrometer within the range of 500–4000 cm^{-1}. Room temperature (300 K, 9.49 GHz) X-band electron paramagnetic resonance (EPR) spectra were performed using a BRUKER EMX 10/2.7 EPR spectrometer consisting of a Bruker ER041XG microwave bridge and field controller and an EMX magnet power supply. Microwave power employed was below saturation levels. The thermogravimetry–differential thermal analysis (TG–DTG curves) was recorded with Netzsch STA 409 Simultaneous Thermal Analyzer in the temperature range RT-800 °C at a rate of 20 °C/min under N_2 atmosphere.

3. Results and discussion

3.1. Optical properties of CdTe@$Cu(OH)_2$ nanocomposite

Fig. 2 shows the absorption spectra and photoluminescence spectra of CdTe nanoparticles before and after coating the $Cu(OH)_2$ shell on CdTe core. The absorption spectra for samples S_1 and S_2 consist of a long wavelength tail bands. The bands were caused by broad size distribution of CdTe@$Cu(OH)_2$ nanocomposite and the intensity of the absorption tail was increased, may

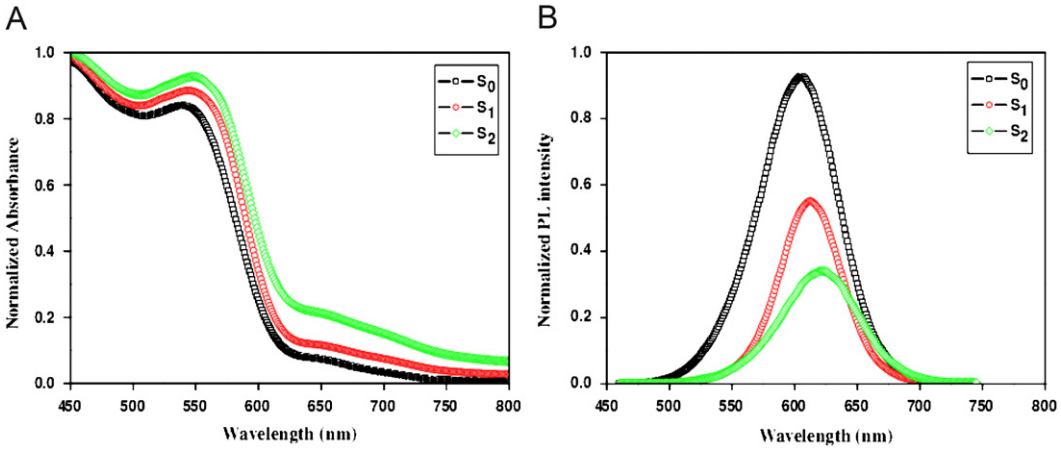

Fig. 2. (A) Absorption and (B) Photoluminescence spectra of MAA-stabilized CdTe nanoparticles (S_0) and CdTe@$Cu(OH)_2$ nanocomposite, (S_1, and S_2).

be due to increasing of the magnetic element concentration (Cu) and refluxing time. With the injection of Cu^{2+} solution to the reactant (CdTe nanocrystals) and further refluxing, the absorbance of the reaction solution increased and shifts to longer wavelength. The PL emission of the reaction solution redshift slightly to longer wavelength and the PL intensity is significantly quenched by adding more amounts of the magnetic metal ions. The surface of the nanocrystals consists of a finite number of binding sites [19], so the rate of binding of ions on the surface of nanocrystals will be decreased with increasing concentration of magnetic metal ions (Cu^{2+}). The redshift and quenching phenomenon are possibly attributed to the effective electron transfer from MAA to magnetic metal ions (Cu^{2+}). The carboxyl groups on the CdTe nanocrystal surface can coordinate with magnetic metal ion (Cu^{2+}) sites, which is responsible for the redshift of the PL spectra of nanocomposites [3,4,20]. Typically, after two-times addition of Cu^{2+} solution and refluxing, the emission peak of the resulted composite nanoparticles (S_2) shifted from 605 nm (S_0) to 621 nm for CdTe@$Cu(OH)_2$ nanocomposites. The absorption and emission of the crude CdTe solution without adding metal cation also shifts to longer wavelength with refluxing because of the growth of CdTe nanocrystals, but the redshift was negligible compared to the shift by adding Cu^{2+}. So the larger redshift after the coating of the magnetic metal hydroxide cannot be due to the growth of CdTe nanocrystals. Furthermore, the redshift of emission was larger than that of absorption, which led to the Stokes shift that became larger (Fig. 3) with the addition of Cu^{2+} and refluxing. The Stokes shift observed for the sample S_0 (emission at 605 nm), S_1 (emission at 612 nm), and S_2 (emission at 621 nm) were 64, 67, 72 nm, respectively. FWHM (the full width at half maximum) of the band-edge luminescence for all samples was from 50 nm to 65 nm, which indicate the narrow size distribution of the as-prepared CdTe nanoparticles and CdTe@$Cu(OH)_2$ nanocomposites[21].

3.2. Structural and compositional analysis of CdTe@$Cu(OH)_2$ nanocomposite

Fig. 4 shows XRD pattern obtained from the CdTe seeds and the core–shell samples with $Cu(OH)_2$ shell. The intensities of the peaks on the XRD pattern of the core–shell samples were weaker than that of "bare" CdTe nanocrystals, and slightly shift to larger angle. In the present work, Cu^{2+} could exchange Cd^{2+} from the surface of CdTe nanocrystals and gets doped in CdTe nanocrystals. This may result in redshift of absorption and emission spectra and the changes in XRD pattern of the (core–shell) nanoparticles. The crystallite size, D_{XRD}, was further estimated from XRD pattern by determining the full-width-half-maximum (FWHM)

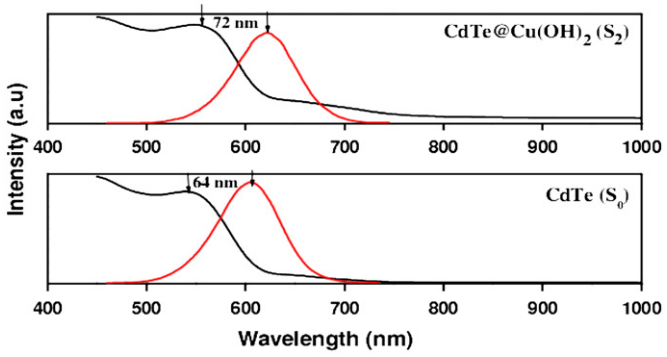

Fig. 3. The Stokes shift of CdTe nanocrystals and CdTe@$Cu(OH)_2$ Nanocomposites, (CdTe: emission at 605 nm, CdTe@$Cu(OH)_2$: emission at 621 nm).

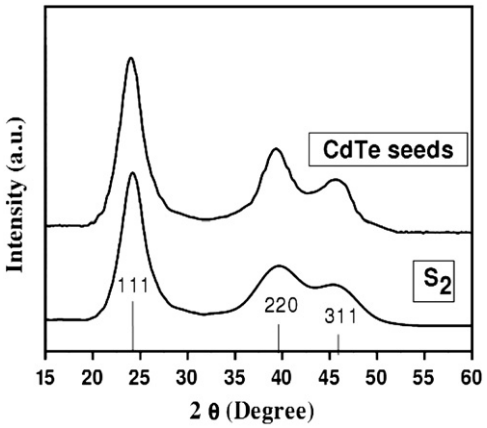

Fig. 4. The XRD patterns obtained from CdTe@$Cu(OH)_2$ powders and their corresponding CdTe seeds.

of characteristic peak (1 1 1), and utilizing the Debye–Scherrer equation for determining the radius of nanoparticles (spherical particles) [22]

$$L = \frac{0.9\lambda}{B\cos\theta} \quad (1)$$

where L is the coherence length, B is the full width at half maximum of the peak, λ is the wavelength of X-ray radiation (1.5406 Å in this study), and θ is the angle of diffraction for (1 1 1) plane. In case of a small crystallites; $L = 3/4D$, where D is diameter of nanoparticles. The size of CdTe nanoparticles were averaged about 3.22 nm, and the CdTe@$Cu(OH)_2$ nanocomposite were averaged as 4.94 nm. The particles with hydroxide shell were bigger than the uncoated CdTe seeds.

Energy-dispersive X-ray analysis (EDAX) spectrum of CdTe@-$Cu(OH)_2$ nanocomposite was shown in Fig. 5. Fig. 5 indicates the presence of Cu and O in these nanoparticles, in addition to Cd, Te, and S. Presence of Cd and Te were from CdTe, Cu and O were from the coating of shell, and S may be from the stabilizer (MAA).

Fig. 6(A) and (B) shows the TEM image and the distribution size diagram of the CdTe nanocrystals and CdTe@$Cu(OH)_2$ composite nanoparticles, respectively. The particles were separately dispersed on a Cu grid and transmission electron microscopy (TEM) investigations were analyzed. TEM image of CdTe nanocrystals revealed crystalline, free-standing, and approximately spherical particles. The sizes of CdTe nanocrystals were averaged about 3.43 nm, and the CdTe@$Cu(OH)_2$ nanocomposite were averaged about 5.19 nm. The size of the particles were almost the same as the average particle size calculated from the Debye–Scherrer equation (3.22 and 4.94 nm for CdTe nanoparticles and the CdTe@$Cu(OH)_2$ nanocomposites, respectively).

3.3. Thermal analysis

Typical TG–DTG curves of the CdTe and CdTe@$Cu(OH)_2$ nanoparticles were measured under an N_2 atmosphere during heating and are shown in Fig. 7(A) and (B). The thermogravimetric pattern of CdTe nanoparticles (Fig. 7(A)) exhibit two evident weight-loss steps; the first weight-loss step below 100 °C was due to removal of various types of water, this corroborates the existence of –OH stretching that was confirmed with FT-IR studies (Fig. 8) and the second weight-loss above 500 °C possibly may be due to the decomposition of Cd–MAA complexes. The thermal behavior of CdTe@$Cu(OH)_2$ was different from that of CdTe seeds, and their DTG curves (Fig. 7(B)), have an additional endothermic peak

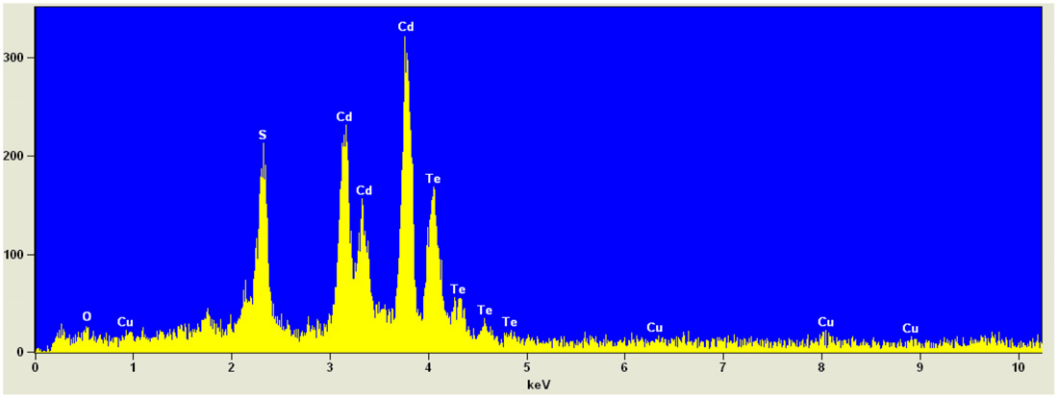

Fig. 5. The EDAX spectrum of CdTe@Cu(OH)$_2$ (core–shell) composite nanoparticles.

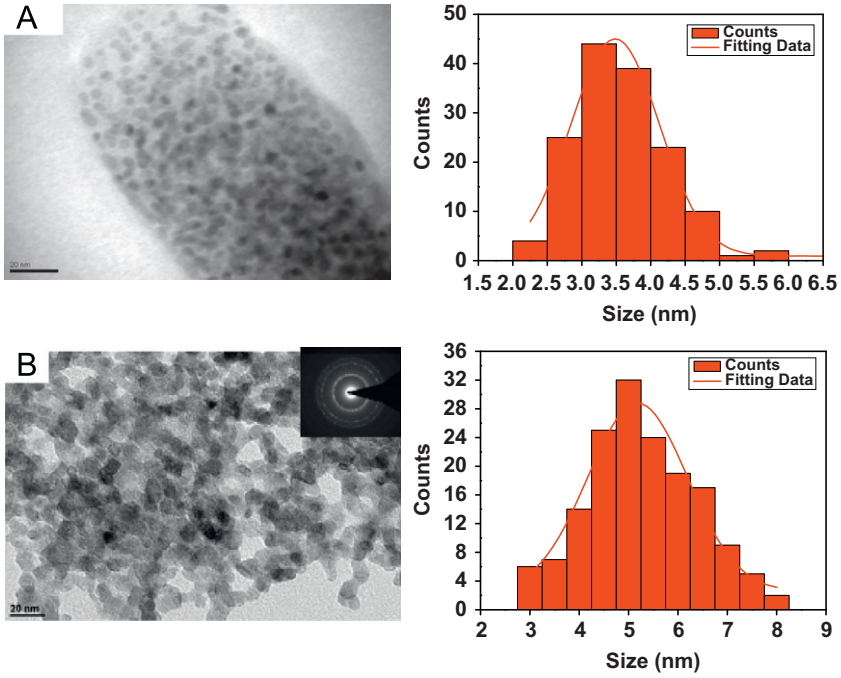

Fig. 6. The TEM image and size dispersion histogram of (A) The CdTe nanoparticles and (B) CdTe@Cu(OH)$_2$ nanocomposite.

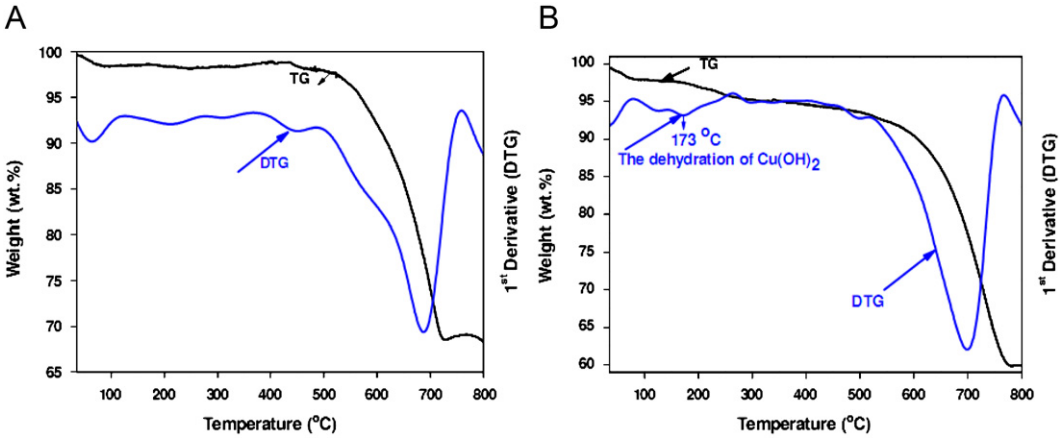

Fig. 7. DTG and TG data of bare core CdTe nanocrystals (A) and CdTe@Cu(OH)$_2$ composite nanoparticles (B).

between 170 and 300 °C, with respect to Cu(OH)$_2$. There is an endothermic peak below 200 °C, may be due to the loss of water produced by dehydration of the copper hydroxide and formation of CuO (Fig. 7(B)) [23–25]. Based on the above analysis and also from the chemistry of copper hydroxides, it was concluded that Cu exists in the composite nanomaterials as Cu(OH)$_2$.

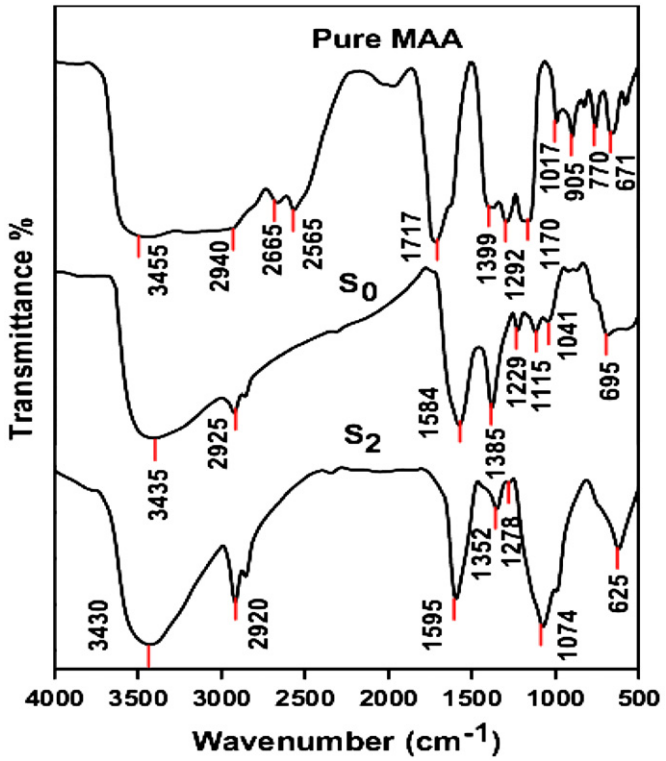

Fig. 8. FT-IR spectrum of pure MAA, (S_0) CdTe nanoparticles capped with MAA, and (S_2) CdTe@Cu(OH)$_2$ composite nanoparticles.

Table 1
Assignment of IR spectra recorded for pure MAA, S_0, and S_2.

Frequency wavenumber (cm^{-1})			Functional group/assignment
Pure MAA	Samples		
	S_0	S_2	
671	695	625	ν(C–S)
1292	1229	1278	((C–O) stretching vibration)
1399	1385	1352	ν_s(COO$^-$)
–	1584	1595	ν_{as}(COO$^-$)
2940	2925	2920	ν(CH$_2$)
3455	3435	3430	OH stretching vibration
1717	–	–	ν(C=O)
2565 and 2665	–	–	The S–H vibrations

3.4. FT-IR spectral analysis

The adsorption of thiols on surface of CdTe and CdTe@Cu(OH)$_2$ nanoparticles were investigated by FT-IR spectral analysis. The FT-IR spectrum of the pure mercaptoacetic acid, mercaptoacetic acid capped CdTe nanoparticles and CdTe@Cu(OH)$_2$ composite nanoparticles was shown in Fig. 8 and their respective infrared absorption bands were tabulated in Table 1.

Table 1 indicates that; the broad peaks observed at around 3430, 3435, and 3455 cm^{-1} in the spectra, may be due to the effect of –OH stretching vibration. The active mode peaks of CH$_2$ (2940 cm^{-1}) in the capped layer were shifted to lower frequency with respect to that of MAA. The shift in CH$_2$ vibrations to smaller frequency indicates that the surfactant molecules in the adsorbed state are affected by the field of solid surface [26]. The S–H vibration bands located at around 2565 and 2665 cm^{-1} in the spectrum of pure mercaptoacetic acid were disappeared completely in the IR spectrum of bare core CdTe nanocrystals and CdTe@Cu(OH)$_2$ composite nanoparticles (S_0 and S_2 in Fig. 8). The vibration band of C=O at around 1717 cm^{-1} in the spectrum of mercaptoacetic acid shifts to 1584 and 1595 cm^{-1} for S_0 and S_2, respectively. These results imply that the mercaptoacetic acid was chemically modified on the surface of CdTe nanoparticles and the COOH was in a state of COO$^-$, making it possible to use the surface-modified CdTe nanoparticles as an analogous polyanionic compounds in the molecular deposition process. The appearance of the bands at 1584 cm^{-1} and 1385 cm^{-1} for S_0, which are attributed to asymmetric ν_{as}(COO$^-$) and symmetric ν_s(COO$^-$) vibration, respectively [27] for the CdTe nanoparticles indicate that MAA is chemisorbed as carboxylate onto Cd ions on CdTe nanoparticles surface. The carboxylic acid was known to be absorbed on metal as carboxylate after deprotonation [28,29].

3.5. EPR analysis

EPR spectra of CdTe and CdTe@Cu(OH)$_2$ (core–shell) composite nanoparticles were obtained using a BRUKER EMX 10/2.7 EPR spectrometer in the range of 2000–4500 Gauss with 9.49 GHz (frequency of the microwave). The magnetic field was modulated at 100 kHz. The spectra were collected using 3.196 mW power and kept at this value to avoid saturation of signals. Measurements were taken at room temperature (300 K). The existence of trace amounts of Cu^{2+} in the CdTe@Cu(OH)$_2$ nanocomposites was confirmed by EPR spectra (Fig. 9).

The g-factor was determined by measuring the field and the frequency at which the resonance occurs and using the relation

$$h\nu = g\beta H \quad (2)$$

where β is the Bohr magnetron ($\beta = 9.274078 \times 10^{-24}$ J/T), g denotes a constant (g factor), h stands for the Plank constant ($h = 6.626176 \times 10^{-34}$ J s), ν is the electromagnetic radiation frequency, and H is the magnetic field strength.

Knowledge of the g-value was used to understand the paramagnetic center's electronic structure. An unpaired electron responds not only to the applied magnetic field H, but also to any local magnetic fields of atoms or molecules. The g-factor value should be equal to the quantity $g_e(1-\sigma)$, where σ includes the effects of local fields (σ can be positive or negative). If g does not equal to g_e, the implication is that the ratio of the unpaired electron's spin magnetic moment to its angular momentum differs from the free electron value. Since an electron's spin magnetic moment may be constant (approximately the Bohr magnetron, β), then the electron must have gained or lost angular

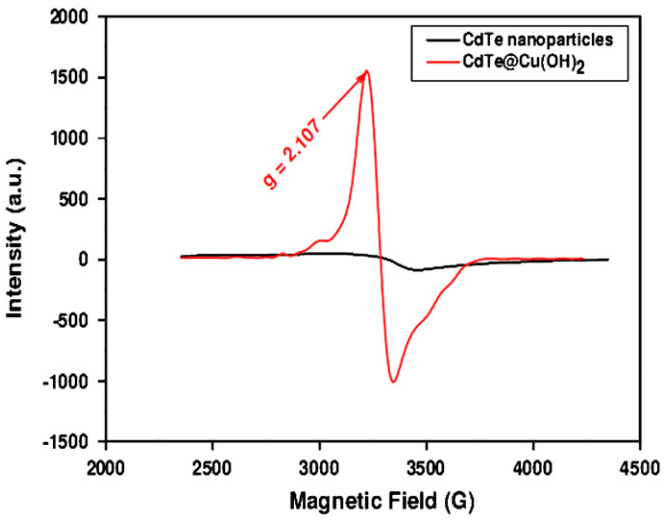

Fig. 9. EPR spectra (9.49 GHz) of CdTe nanoparticles capped with MAA, and CdTe@Cu(OH)$_2$ nanocomposite.

momentum through spin–orbit coupling. Since, the mechanism of spin–orbit coupling was well known; the magnitude of the change gives information about the nature of the atomic or molecular orbital containing the unpaired electron.

Fig. 9 indicates that all samples have sharp and broad signals at different *g*-values and the concentration of paramagnetic center's vary with the samples. The EPR spectrum of capped-CdTe nanocrystals (Fig. 9) indicate the resonance position corresponding to a *g*-factor of 2.093, close to that of the free electron value of $g_e=2.002$. The spectrum was attenuated upon purification by size-selective precipitation. Assuming that the impurity was spin 1/2, comparison with an external standard showed that the total impurity concentration to be approximately 1 per nanocrystal in samples, size selected once, and approximately to be 0.1 per nanocrystals in samples, size selected three times. The intensity of the impurity signal gets decreased on subsequent mecraptoacetic Acid (MAA) cap exchange with CdTe nanocrystals. Other than the fact that they are surface related, this signal could not be assigned. A typical EPR spectrum of CdTe@$Cu(OH)_2$ nanocomposites with averaged size of 4.94 nm indicates the resonance position for the sharp spectrum with the band width 13 mT corresponding to a *g*-factor of 2.107. This *g*-factor was shifted very much from that of the free electron value of $g_e=2.002$ and also from the *g*-value of capped-CdTe nanocrystals. The shift of *g*-values was attributed for paramagnetic transition metal ions (Cu^{2+}).

4. Conclusion

CdTe@$Cu(OH)_2$ nanocomposites were synthesized based on a seed-mediated growth approach, composed of a fluorescent nanocrystals core, CdTe, and a magnetic metal hydroxides, $Cu(OH)_2$. The fluorescent CdTe nanoparticles were used as a core and then shell layer of magnetic hydroxides were formed on it. The synthetic procedure is simple, and can be easily scaled up. Wide angle X-ray diffraction was used to probe the internal structure of the nanoparticles and indicates that the coverage of CdTe nanoparticles by magnetic hydroxides shell. The size of CdTe nanoparticles was averaged about 3.22 nm, and the size of CdTe@$Cu(OH)_2$ (core–shell) composite nanoparticles were averaged 4.94 nm, respectively. The EDAX (energy-dispersive X-ray Analysis) results indicate the presence of Cu and O in these nanoparticles as well as Cd, Te and S. The Cd and Te were from CdTe nanoparticles, Cu and O were from the respective shell, and the S was attributed to the stabilizer of (mercaptoacetic acid, MAA). TEM images demonstrated homogeneous size distribution for these (core–shell) nanoparticles and the size of the (core–shell) nanoparticles were evaluated. Both absorption and PL spectra exhibit "quantum size effects" and depending on the thickness of the hydroxide shell. The observed red-shift rules out the formation of an alloy of the core and shell materials and indicated that the growth is controlled. From the FT-IR Spectra it is concluded that the nanoparticles were adsorbed by the –SH groups and the free carboxylic acid group exists as carboxylate ion and make the capped particles soluble in water. The EPR spectrum confirms the presence of magnetic particles as shell in the nanoparticles.

Acknowledgements

The authors sincerely thank DST, GOVT. of INDIA (DST/TSG/PT/2008/15) for funding the research forming part of the paper. One of the authors (Dr. M. S. Abd El-sadek) sincerely thanks ICCR, Govt. of India for the fellowship.

References

[1] G. Rupali, D. Amitabha, Chem. Mater. 12 (2000) 608.
[2] L.L. Beecroft, C.K. Ober, Chem. Mater. 9 (1997) 1302.
[3] M.S. Abd El-sadek, J. Ram kumar, S. Moorthy Babu, M. Salim El-Hamidy, J. Alloys Compd. 496 (2010) 589.
[4] M.S. Abd El-sadek, J. Ram kumar, S. Moorthy Babu, M. Salim El-Hamidy, Mater. Chem. Phys. 124 (2010) 592.
[5] E.E. Carpenter, C. Sangregorio, C.J. O'Connor, IEEE Trans. Magn. 35 (1999) 3496.
[6] N.S. Sobal, U. Ebels, H. Mohwald, M. Giersig, J. Phys. Chem. B 107 (2003) 7351.
[7] T. Ung, L.M. Liz-Marzan, P. Mulvaney, J. Phys. Chem. B 103 (1999) 6770.
[8] G. Oldfield, T. Ung, P. Mulvaney, Adv. Mater. 12 (2000) 1519.
[9] H. Kim, M. Achermann, L.P. Balet, J.A. Hollingsworth, V.I. Klimov, J. Am. Chem. Soc. 127 (2005) 544.
[10] L. Li, J. Ren, J. Solid State Chem. 179 (2006) 1814.
[11] G.H. Du, T.G. Van, Chem. Phys. Lett. 393 (2004) 64.
[12] C.H. Lu, L.M. Qi, J.H. Yang, D.Y. Zhang, N.Z. Wu, J.M. Ma, J. Phys. Chem. B 108 (2004) 17825.
[13] X.Y. Song, S.X. Sun, W.M. Zhang, H.Y. Yu, W.L. Fan, J. Phys. Chem. B 108 (2004) 5200.
[14] X.G. Wen, W.X. Zhang, S.H. Yang, Z.R. Dai, Z.L. Wang, Nano Lett. 2 (2002) 1397.
[15] X.G. Wen, W.X. Zhang, S.H. Yang, Langmuir 19 (2003) 5898.
[16] S.H. Park, H.J. Kim, J. Am. Chem. Soc. 126 (2004) 14368.
[17] X. Wu, H. Bai, J. Zhang, F. Chen, G. Shi, J. Phys. Chem. B 109 (2005) 22836.
[18] M.S. Abd El-sadek, S. Moorthy Babu, Physica B 405 (2010) 3279.
[19] W.S. Brey, Physical chemistry and its biological applications, Academic Press, New York, 1978 Chapter 9.
[20] K. Youngjin, C.J. Robert, T.H. Joseph, Nano Lett. 1 (2001) 165.
[21] L. Li, H. Qian, J. Ren, Chem. Commun. 32 (2005) 4083.
[22] A. Guinier, X-Ray Diffraction: In Crystals, Imperfect Crystals, and Amorphous Bodies, W. H. Freeman & Company, San Francisco, USA, 1963 Chapter 2 p. 49.
[23] J.R. Gunter, H.R. Ostwald, J. Appl. Cryst. 3 (1970) 21.
[24] M.N. Kopylovich, A.M. Kirillov, A.K. Baev, Russ. J. Appl. Chem. 74 (2001) 12.
[25] Y. Cudennec, A. Lecerf, Solid State Sci. 5 (2003) 1471.
[26] S. Wageh, Physica E 39 (2007) 8.
[27] N.B. Colthup, L.H. Daly, S.E. Wiberley, Introduction to Infrared and Raman Spectroscopy, 3rd Edn., Hacourt Brace Jovanovich, New York, 1990, p. 291.
[28] S.W. Han, H.S. Han, K. Kim, Vib. Spectrosc. 21 (1999) 133.
[29] Y.T. Tao, J. Am. Chem. Soc. 115 (1993) 4350.